EARTHQUAKE ENGINEERING AND STRUCTURAL DYNAMICS
*Earthquake Engng Struct. Dyn.* 2000; **29**: 603–627

# VFPI: an isolation device for aseismic design

M. Pranesh* and Ravi Sinha

*Department of Civil Engineering, Indian Institute of Technology, Powai, Mumbai 400 076, India*

SUMMARY

Sliding isolators with curved surface are effective base isolation systems incorporating isolation, energy dissipation and restoring mechanism in one unit. However, practical utility of these systems, such as friction pendulum system (FPS) has limitations due to constant isolator period and restoring force characteristics. A new isolator called the variable frequency pendulum isolator (VFPI) that overcomes these limitations while retaining all the advantages has been described in this paper. VFPI has oscillation frequency decreasing with sliding displacement, and the restoring force has an upper bound so that the force transmitted to the structure is limited. The mathematical formulations for the response of a SDOF structure and energy balance are also described. Parametric studies have been carried out to critically examine the behaviour of structures isolated with VFPI, FPS and PF system. From these investigations, it is concluded that the VFPI combines the advantages of both FPS and PF system, without their undesirable properties. The VFPI performance is also found to be stable during low-intensity excitations, and fail-safe during high-intensity excitations. VFPI is found to exhibit robust performance for a wide range of structure, isolator and ground motion characteristics clearly demonstrating its advantages. Copyright © 2000 John Wiley & Sons, Ltd.

KEY WORDS: structural control; base isolation; energy dissipation; earthquake engineering; passive control; VFPI

## 1. INTRODUCTION

One of the most effective techniques for aseismic design of structures is to control the energy that is transmitted from the ground or foundation to the structure. This is generally achieved by introducing a flexible layer (or isolator) between the superstructure and the foundation, thereby shifting the fundamental period of the structure away from the predominant periods of the input excitation. Base isolation systems have been used extensively for mechanical systems where the excitation is often well defined and periodic (see, for example, Snowdem [1]). The extension of base isolation concepts to Civil Engineering structures is relatively new. Extensive reviews of base isolation for Civil Engineering structures, discussing the different types of isolation systems and their applicability, have been provided by Kelly [2, 3] and Buckle and Mayes [4].

* Correspondence to: Ravi Sinha, Department of Civil Engineering, Indian Institute of Technology, Powai, Mumbai 400 076, India.



*Received 18 July 1999*
*Accepted 12 October 1999*

In order to reduce deformations at the isolator level, most modern isolation devices integrate both the flexible layer as well as energy dissipating mechanism into a single system. For example, friction type base isolator, in which a sliding surface is used for isolation, is very effective in reducing structural response and incorporating isolation and energy dissipation in one unit [5]. Owing to the characteristics of the excitation transmitted through the sliding surface, the performance of friction isolators is quite insensitive to severe variations in the frequency content and amplitude of the input excitation, making them very robust [6]. However, the simple sliding isolator consisting of horizontal sliding surface (pure-friction system) may result in large sliding and residual displacements, which may be difficult to incorporate in structural design. The practical effectiveness of friction isolators can be enhanced by adding a suitable restoring mechanism and thereby reducing the residual displacements to manageable levels. Several systems have been suggested in the past to accommodate restoring mechanism in a structure isolated by sliding system. In some sliding isolation structures, the re-centring mechanism takes the form of cylindrical rubber springs [7–9]. In another system, the restoring mechanism has been provided by rubber bearings [10]. Similarly, the central and the peripheral rubber cores in resilient-friction base isolation (R-FBI) system provide restoring mechanism [11].

An interesting isolation device named as friction pendulum system (FPS) provides restoring mechanism by gravity [12, 13]. In this system the sliding and re-centring mechanisms are integrated in one unit in which the sliding surface takes a spherical shape (Figure 1). The effectiveness of FPS isolator has been widely investigated both analytically and experimentally, and it has been found suitable for many different structures and excitation characteristics [14–17]. Unified equations of motion for the analysis of FPS isolators in both stick and slip phases have been recently proposed to simplify the highly non-linear analysis procedure [18]. A historic building in San Francisco that suffered damage during the 1989 Loma Prieta earthquake has been recently retrofitted using FPS isolators [19].

The sliding surface of FPS isolator is spherical so that its time period of oscillation remains constant. Unfortunately, the use of spherical sliding surface results in several practical disadvantages. One main disadvantage is that FPS needs to be designed for a specific level (intensity) of ground excitation. This is primarily because the maximum intensity of excitation has a strong influence on FPS design, even though the performance of structures isolated by FPS is relatively independent of the frequency content of ground motion. In general, FPS designed for a particular intensity of excitation may not give very satisfactory performance during earthquakes with much lower or higher intensity [20].

In the present paper, a new isolation system called *variable frequency pendulum isolator* (VFPI) has been proposed. In this isolator, the shape of the sliding surface is non-spherical. This isolation system retains the advantages of both the pure friction (PF) isolation system and FPS, due

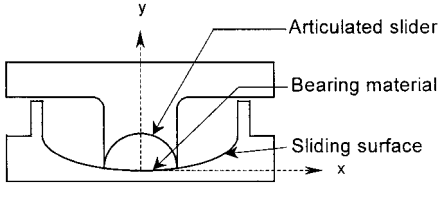


Figure 1. Schematic diagram of curved sliding-surface isolator.

 

to amplitude dependent time-period and softening mechanism of isolator restoring force. The geometry of the isolator can be chosen to achieve a progressive period shift at different response levels. Mathematical formulation similar to that of a PF system has been developed for the response of structures isolated by VFPI. Energy formulation is also developed to substantiate the results and improve the understanding of isolator performance.

The response of single-storey example structures isolated by VFPI has been investigated to study its effectiveness under earthquake excitation. The results are compared with the response using FPS and PF isolators for the same structures. The influence of shifting of oscillation period and softening mechanism of restoring force on the fail-safe characteristic for the proposed isolator has also been investigated. The influence of different parameters of VFPI on the response has also been investigated through parametric studies.

## 2. SLIDING SURFACE GEOMETRY

### *2.1. Background*

The isolator force of a sliding isolator consists of two main components, namely, the restoring force (RF) due to the component of the self-weight tangent to sliding surface, and the frictional force (FF) opposing the sliding. The self-weight always contributes towards the restoring mechanism and is directed towards the initial position. The direction of friction force is opposite to the direction of sliding, and may contribute to or resist the restoring force. The total isolator force (RF + FF) is a useful parameter to characterise the performance of a friction isolator. In case of a PF system, the restoring force is zero and the response is wholly governed by the friction force, thereby restricting the maximum transmitted acceleration to the product of coefficient of friction and gravitational acceleration, $\mu g$.

In friction pendulum system (FPS) the restoring force varies linearly with sliding displacement, so that the isolator force increases with sliding displacement. Depending on the direction of sliding, restoring force (RF) and frictional force (FF) are additive or subtractive. As the value of RF is usually negligible for small sliding displacements, the isolator behaviour is almost entirely governed by the value of FF for low and medium level of excitations. The FPS performance is thus similar to a pure friction system, and is also nearly independent of frequency content of the excitation. However, for high-intensity excitation (causing relatively large sliding displacements), the RF may be significantly larger than FF. As a result, response of the structure may be dependent on the frequency content and amplitude of excitations, severely affecting the isolator effectiveness. If the coefficient of friction is low, the problem may be further aggravated due to large sliding displacement even for moderate intensity ground excitations. It can be concluded that the linear force–deformation relation of FPS makes the effectiveness of isolator low, particularly for high-intensity earthquake motions or low coefficient of sliding friction.

A new isolator sliding surface geometry has been developed that gives performance similar to that of FPS for low levels of excitation and similar to that of pure friction system for high level of excitation. This is achieved by making the oscillation frequency of the isolator response dependent. The isolator geometry is such that its frequency decreases with increase in sliding displacement and asymptotically approaches zero (PF system) at very large displacement. This results in continuous variation of oscillation frequency even for high level of excitation and the isolation always remains effective. An additional important property is that the restoring force has an

 

upper bound, and it decreases for larger sliding displacement thereby provides force-softening mechanism. As the magnitude of force transmitted at higher level of excitations is small compared to FPS, this system also allows use of surfaces with low coefficient of friction. This isolation system thus differs from the conventional PF and FPS systems in two fundamental properties: (1) VFPI provides for progressive period lengthening mechanism that is dependent on sliding displacement; and (2) VFPI permits softening of restoring force at large displacement so that the energy dissipation characteristics of the isolator are superior to that of currently available isolators.

### 2.2. Mathematical model

Consider a rigid block of mass $m$ sliding on a curved surface of any geometry, $y = f(x)$ (Figure 2). At any instant the restoring force is given by

$$f_R = mg \frac{dy}{dx} \tag{1}$$

Assuming that the restoring force mechanism is mathematically represented by an equivalent non-linear spring, the spring force can be expressed as the product of the equivalent spring stiffness and the deformation:

$$f_R = k(x)x \tag{2}$$

where $k(x)$ is the non-linear spring stiffness, and $x$ is the displacement of the mass. If the isolator is modelled as a single-degree-of-freedom oscillator, the spring force (restoring force) can be expressed as the product of the total mass of the system and square of oscillation frequency as

$$f_R = m\omega_b^2(x)x \tag{3}$$

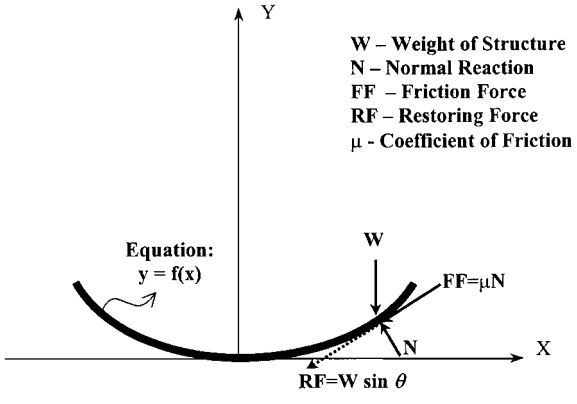


Figure 2. Free body diagram of sliding surface of isolator showing forces at point of contact.

 

Here, $\omega_b(x)$ is the instantaneous isolator frequency, and depends solely on geometry of the sliding surface. In case of a conventional FPS with spherical sliding surface, this frequency is almost constant and is equal to $\sqrt{g/R}$, where $R$ is the radius of curvature of the sliding surface [13]. By substituting this in Equation (3), it can be easily seen that the restoring force is a linear function of the sliding displacement.

The definition of oscillation frequency at any displacement $x$ is geometrically equivalent to placing a spherical surface of suitable radius of curvature through that point with centre of the surface on the vertical axis of the isolator. This simple geometrical interpretation of the sliding surface has been extended to develop isolators with the desired variation in its frequency and restoring force.

*2.2.1. Proposed geometry.* It has been found that a standard second-degree curve to represent sliding surfaces such as sphere, ellipse, hyperbola and parabola cannot provide the required variation of isolator frequency and restoring force [21]. However, sliding surface based on the expression of an ellipse can be used to develop the isolator with desired properties. The equation of an ellipse with $a$ and $b$ as its major and minor axes, respectively, and with co-ordinate axes as shown in Figure 2 is given by

$$y = b\,(1 - \sqrt{1 - x^2/a^2}) \tag{4}$$

Differentiating with respect to $x$, the slope at any point on the curve is given by

$$\frac{\mathrm{d}y}{\mathrm{d}x} = \frac{b}{a^2\sqrt{1 - x^2/a^2}}\,x \tag{5}$$

If the equation of the sliding surface is represented by Equation (4), the frequency of the isolator can be determined by substituting Equations (4) and (5) into (1) and (3), and the final expression is

$$\omega_b^2(x) = \omega_I^2/\sqrt{1 - x^2/a^2} \tag{6}$$

where $\omega_I^2 = gb/a^2$ is the square of initial frequency of the isolator (at zero displacement). It can be seen that the frequency of an elliptical curve is fairly constant for small displacements ($x \ll a$) and this value depends on the ratio $b/a^2$.

In the proposed isolator geometry of VFPI, the major axis of the ellipse, $a$, is taken as a linear function of the sliding displacement, $x$. This is geometrically equivalent to an infinite number of progressively larger ellipses transforming into one another with increase in sliding displacement. At very large sliding displacement ($x \to \infty$), the frequency approaches zero. In the present formulation, the major axis has been expressed as

$$a = x + d \tag{7}$$

where $d$ is a constant. Substituting in Equation (4), the expression for ellipse can be simplified as

$$y = b\left[1 - \frac{\sqrt{d^2 + 2dx\,\mathrm{sgn}(x)}}{d + x\,\mathrm{sgn}(x)}\right] \tag{8}$$

 

where sgn $(x)$ is the signum function which assumes a value of $+1$ for positive sliding displacement and $-1$ for negative sliding displacement. The signum function has been introduced to maintain symmetry of sliding surface about the vertical axis.

It can be observed that this equation gives an upper bound on the vertical displacement, $b$, occurring only at infinitely large sliding displacement. Now, by differentiating, the slope at any point on the sliding surface is given as

$$\frac{\mathrm{d}y}{\mathrm{d}x} = \frac{bd}{(d + x\,\mathrm{sgn}\,(x))^2\sqrt{d^2 + 2dx\,\mathrm{sgn}\,(x)}}\,x \tag{9}$$

To simplify the notations, a non-dimensional parameter $r = x\ \mathrm{sgn}\,(x)/d$ has been introduced. By substituting $r$ and the initial frequency $\omega_\mathrm{I}^2 = gb/d^2$ in Equation (9), and combining with Equations (1) and (3), the isolator frequency at any sliding displacement can be expressed as

$$\omega_\mathrm{b}^2(x) = \frac{\omega_\mathrm{I}^2}{(1 + r)^2\sqrt{1 + 2r}} \tag{10}$$

In the above equations, parameters $b$ and $d$ completely define the isolator characteristics. It can be observed that the ratio $b/d^2$ governs the initial frequency of the isolator. Similarly, the value of $1/d$ determines the rate of variation of isolator frequency, and this factor has been defined as *frequency variation factor* (FVF). It can also be seen from Equation (10) that the rate of decrease of isolator frequency is directly proportional to the FVF for a given initial frequency. The variation of oscillation frequency of a typical VFPI with respect to the sliding displacement is shown in Figure 3(a). For comparison purposes, the oscillation frequency of FPS with same initial

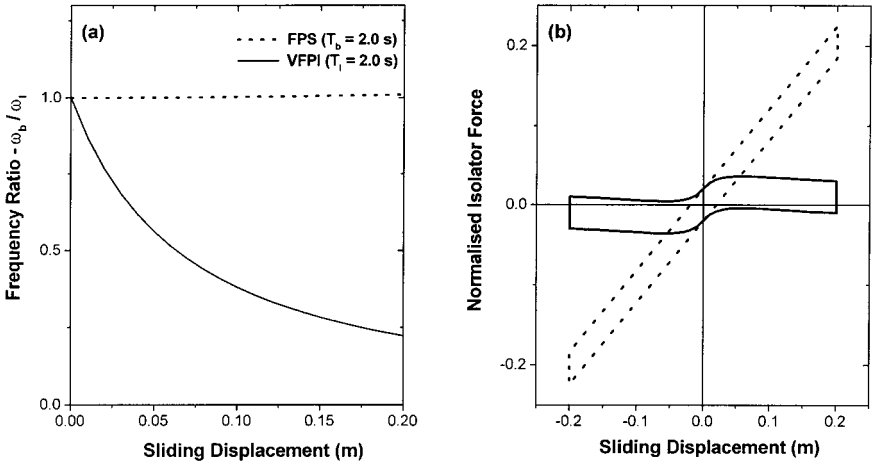


Figure 3. Frequency and restoring force characteristics of VFPI and FPS ($\mu = 0.02$, VFPI: $d = 0.3$ m, $b = 0.09$ m; FPS: $R = 1$ m).

 

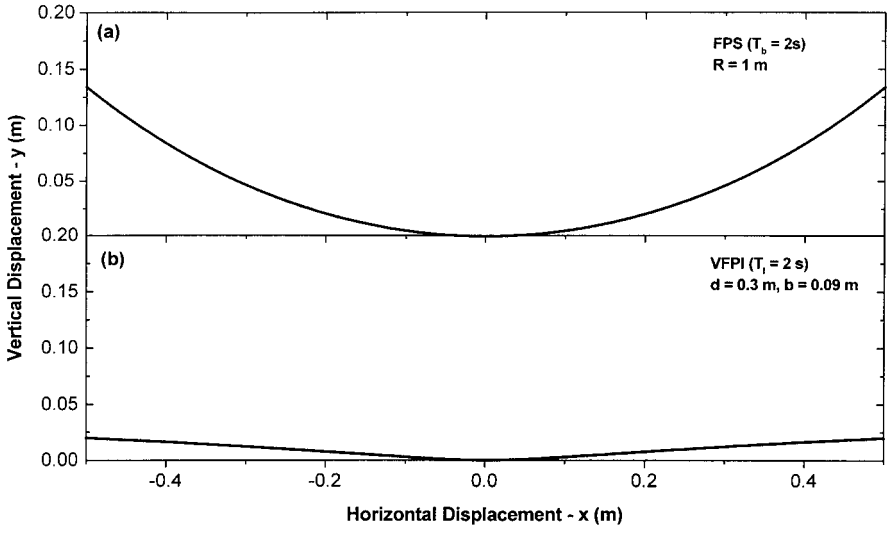


Figure 4. Shape of sliding surface of FPS and VFPI.

frequency has also been plotted, which has been found to be almost constant. From this plot it is seen that the oscillation frequency of VFPI sharply decreases with increasing sliding displacement and asymptotically approaches zero.

The variation of restoring force [Equation (1)] with sliding displacement for the example FPS and VFPI are shown in Figure 3(b). In this plot, the restoring force has been normalized with respect to *mg*. It can be observed that the isolator force in VFPI first increases to reach its maximum value and later slowly decreases so as to asymptotically approach the frictional force. Further, for very small displacements the restoring force variation is approximately linear. In FPS, on the other hand, the restoring force varies linearly with sliding displacement. From this it can be expected that the VFPI behaviour is similar to that of FPS for small displacements (with desired high initial stiffness) and its behaviour is similar to PF system for very large displacements. It is therefore possible to design VFPI with suitable properties so that the isolator derives the advantages of both FPS and PF at different excitation levels.

The sliding surface of the example VFPI and FPS has been shown in Figure 4. It can be observed that VFPI is relatively flatter than FPS, which results in smaller vertical displacement for similar sliding displacements [20]. This is an additional advantage of VFPI compared to FPS since flatter sliding surface will result in the generation of smaller overturning forces in the structure.

## 3. MATHEMATICAL FORMULATION

Consider a single-degree-of-freedom structure isolated using a curved-surface friction isolator subjected to a horizontal ground excitation $\ddot{x}_g$ (Figure 5). The free-body diagram (FBD) of the sliding surface of the isolator is as shown in Figure 2, which shows the forces acting on the isolator

 

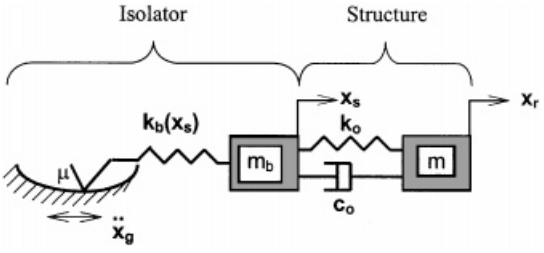


Figure 5. Analytical model of a single storey structure isolated by curved sliding surface isolator.

surface when the sliding is in positive $x$ direction. The mathematical formulation for response of structure has been developed with the following assumptions.

1. The coefficient of friction in static and dynamic conditions is assumed constant, and Coulomb's friction law has been used.
2. The structure has been subjected to horizontal ground motion only and the effect of vertical acceleration due to rising of the structure is neglected.
3. The slider of the isolator is assumed to have point contact with the sliding surface.
4. The overturning effect on the structure due to uneven distribution of normal force at the isolator is neglected.

These assumptions are commonly used for analysis of isolated structures, and do not generally introduce large errors in the response calculations.

### 3.1. *Equations of motion*

The motion consists of two phases namely, non-sliding phase when the structure does not move with respect to the sliding surface, and sliding phase. The equations of motion are different in the two phases and the overall behaviour is highly non-linear. The total motion can be considered as a series of non-sliding and sliding phases in succession.

*3.1.1. Non-sliding phase.* In this phase the structure behaves as a conventional fixed-base structure. Since the static frictional resistance is greater than the horizontal forces acting on the structure, the base mass does not move relative to the sliding surface. The equations of motion governing this phase are

$$\ddot{x}_r + 2\xi_0\omega_0\dot{x}_r + \omega_0^2 x_r = -\ddot{x}_g \tag{11}$$

$$\ddot{x}_s = \dot{x}_s = 0 \quad \text{and} \quad x_s = \text{constant} \tag{12}$$

where $x_r$ is the relative displacement of the top mass with respect to the base mass, $x_s$ is the sliding displacement of the base mass relative to the ground, overdot indicates the derivative with respect to time, and $\omega_0 = \sqrt{k_0/m}$ and $\xi_0 = c_0/2\sqrt{k_0 m}$ are the frequency and damping ratio, respectively, of the fixed base single degree-of-freedom structure. As the structure is at rest before the application of ground motion, the motion in structure always starts in non-sliding phase.

 

*3.1.2. Initiation of sliding phase.* For the initiation of sliding phase, the absolute value of the sum of total inertia force and restoring force should be greater than or equal to the absolute value of the frictional force acting along the sliding surface. Referring to Figure 2, we can write the condition for start of a sliding phase as

$$|[m\,(\ddot{x}_r + \ddot{x}_g) + m_b\ddot{x}_g]\cos\,\theta + (m + m_b)g\sin\,\theta| \geqslant \mu\,(m + m_b)g\,\cos\,\theta \tag{13}$$

where $\theta$ is the angle of tangent at the point of contact with horizontal and $\mu$ is the coefficient of sliding friction. Now dividing Equation (13) by $\cos\theta$ and substituting $\mathrm{d}y/\mathrm{d}x_s$ for $\tan\theta$, the condition for sliding can be simplified as

$$\left|[m(\ddot{x}_r + \ddot{x}_g) + m_b\,\ddot{x}_g] + (m + m_b)g\,\frac{\mathrm{d}y}{\mathrm{d}x_s}\right| \geqslant \mu(m + m_b)g \tag{14}$$

It can be recalled that $(m + m_b)\,g\;\mathrm{d}y/\mathrm{d}x_s$ is the restoring force for a given sliding displacement [Equation (1)]. If the restoring force is expressed as a product of spring stiffness and sliding displacement, the spring force is given by [Equation (3)],

$$f_R\;=\;(m + m_b)\omega_b^2\,(x_s)x_s \tag{15}$$

where $\omega_b(x_s)$ is isolator frequency and is a function of the sliding displacement. Dividing Equation (14) by the total mass and defining the mass ratio as

$$\alpha = \frac{m}{m + m_b} \tag{16}$$

the condition for initiation of the sliding phase can be simply expressed as

$$|\alpha\ddot{x}_r + \ddot{x}_g + \omega_b^2(x_s)x_s| \geqslant \mu g \tag{17}$$

*3.1.3. Sliding phase.* In this phase the static frictional force is overcome and there is relative motion between the sliding surface and the base mass. During the sliding phase, the structure behaves like a two-degree-of-freedom structure. The equations of motion for the top and bottom mass are, respectively

$$\ddot{x}_r + 2\xi_0\,\omega_0\,\dot{x}_r + \omega_0^2\,x_r = -\,\ddot{x}_s - \ddot{x}_g \tag{18}$$

and

$$\alpha\ddot{x}_r + \ddot{x}_s + \omega_b^2\,(x_s)\,x_s = -\,\ddot{x}_g - \mu g\;\mathrm{sgn}(\dot{x}_s) \tag{19}$$

As discussed above, the isolator frequency, $\omega_b(x_s)$, in Equation (19) depends solely on the geometry of the sliding surface.

*3.1.4. End of sliding phase.* A sliding phase ends when the sliding velocity of the base mass becomes equal to zero, i.e.

$$\dot{x}_s = 0 \tag{20}$$

 

As soon as this condition is satisfied, Equations (11) and (12) corresponding to the non-sliding phase need to be evaluated to further check the validity of the inequality in Equation (17). This decides whether the structure continues in the sliding phase after a momentary stop or enters a non-sliding phase.

*3.1.5. Direction of sliding.* The direction of sliding at the end of any non-sliding phase is decided by the signum function, $\mathrm{sgn}(\dot{x}_s)$. This value is determined from the sign of the sum of total inertia force and isolator restoring force as

$$\mathrm{sgn}(\dot{x}_s) = -\frac{\alpha\ddot{x}_r + \ddot{x}_g + \omega_b^2(x_s)}{|\alpha\ddot{x}_r + \ddot{x}_g + \omega_b^2(x_s)|} \tag{21}$$

The value of signum function during any sliding phase of motion remains constant until the sliding velocity becomes zero. Thereafter, the structure may (i) enter a non-sliding phase, or (ii) reverse its direction of sliding or (iii) and continue in the same direction after a momentary stop. To determine the correct state, the solution process should continue with the equations of non-sliding phase wherein the sliding acceleration is forced to zero and further check for the validity of the inequality (17). If this inequality is satisfied at the same instant of time when the sliding velocity is zero, then Equation (21) decides the further direction of sliding.

### *3.2. Energy formulation*

Most of the base isolators work through a combination of deflecting the seismic energy (reducing the energy transmitted to a structure) and dissipating energy through a suitable mechanism. Base isolation attempts to reduce the structural deformations by allowing relatively large displacements at the isolator level. Isolation systems can sometimes be designed for optimal values of some response quantities; however, it is often very difficult to decide the response quantities for an optimum performance of the isolator. Energy quantities are evaluated using all response quantities, and are thus better indicators of the isolator performance. In view of this energy evaluation in base-isolated structures assumes significance.

When energy is transmitted into an isolated structure due to ground motions, the structure may respond in sliding or non-sliding phases. If the response is non-sliding (like fixed base structure), the entire energy is transmitted into the structure, which results in the development of kinetic, potential and dissipative energy in the structure. When the structure response is in sliding phase, the absolute input energy can be defined in terms of work done by the isolator force (frictional force + restoring force) due to ground displacement. This definition is similar to that proposed by Uang and Bertero [22] for a fixed-base structure. Some portion of the input energy is dissipated due to friction at sliding surface, and the remaining input energy is transmitted to the structure. Out of this total transmitted energy, a portion is dissipated by non-yielding mechanisms usually represented by equivalent viscous damping [23]. The remaining portion consists of the kinetic energy of the top and bottom masses and the potential energy due to structural elastic deformations (elastic strain energy), and that induced by the rising of the structure along the sliding surface.

The energy formulation for a single-storey structure isolated by VFPI is presented in this section. The formulation assumes that the structure response remains elastic throughout the excitation. The 'absolute energy' formulation given by Uang and Bertero [22], has been extended to a single-storey structure isolated by a curved sliding surface.

 

The dynamic equilibrium of the entire structure (Figure 5) gives the following dynamic equilibrium equation:

$$m\ddot{x}_r^t + m_b\ddot{x}_s^t + (m + m_b)\,\omega_b^2(x_s)\,x_s + (m + m_b)\,\mu g\ \mathrm{sgn}(\dot{x}_s) = 0 \tag{22}$$

where, the superscript $t$ indicates the absolute values of the response quantity. Also, from the dynamic equilibrium of the free-body diagram of the top mass, one gets

$$m\ddot{x}_r^t = -c_0\dot{x}_r - k_0 x_r \tag{23}$$

Integrating Equation (22) with respect to the sliding displacement $x_s$, substituting Equation (23) and rearranging the terms we get

$$\tfrac{1}{2}m\dot{x}_r^{t^2} + \tfrac{1}{2}m_b\dot{x}_s^{t^2} + \int (m + m_b)\,\omega_b^2(x_s)\,x_s\,\mathrm{d}x_s + \int c_0\dot{x}_r\,\mathrm{d}x_r + \tfrac{1}{2}k_0 x_r^2 + \int (m + m_b)\mu g\ \mathrm{sgn}(\dot{x}_s)\,\mathrm{d}x_s = \int m\ddot{x}_r^t\ \mathrm{d}x_g + \int m_b\ddot{x}_s^t\ \mathrm{d}x_g \tag{24}$$

The above equation can be written in the following form:

$$E_k^r + E_k^s + E_s + E_{rst} + E_\xi + E_\mu = E_i \tag{25}$$

where $E_k^r$ and $E_k^s$ are the absolute kinetic energies of the top and bottom masses respectively, $E_s$ and $E_{rst}$ are the restorable elastic energy due to structural deformations and potential energy due to rising of the structure along the curved isolator surface, respectively, and $E_\xi$ and $E_\mu$ are the energy dissipated due to viscous damping and sliding friction, respectively. Now, the terms $m\ddot{x}_r^t$ and $m_b\ddot{x}_s^t$ are the inertia forces generated in the structure and the base mass and their sum is equal to the total force at the isolator level (restoring force + frictional force). The term on the RHS side of Equation (24) therefore represents the work done by these on the foundation displacement and is defined as the absolute input energy $E_i$.

### *3.3. Solution of equations of motion and energy evaluation*

The equations are linear in non-sliding phase and non-linear in sliding phase and the overall behaviour is highly non-linear. These equations can be numerically solved using appropriate non-linear solution techniques. As the system is classically damped in non-sliding phase, normal mode method is used in this phase. The system is non-classically damped in sliding phase. However, normal modes can still be used to simplify the procedure [24, 25]. If $n$ superstructure normal modes are considered in the analysis, then complex mode method is applied to a set of $n + 1$ co-ordinates only, the additional co-ordinate corresponding to the base [21]. Furthermore, as the isolation system has non-linear restoring force, the modal properties need to be modified at each time step in the sliding phase. Assuming the ground excitation as a piece-wise linear function, a close-form step-by-step integration procedure has been developed to solve the uncoupled first order differential equations involving the complex modal properties. The final expressions have been presented in Appendix.

 

During the solution of such non-linear equations, accuracy of the result is extremely sensitive to the change in phase of motion from non-sliding to sliding and *vice versa*. As a result, the exact time of change in phase must be determined very accurately. In the present investigation, this is taken care of by subdividing the chosen time interval further whenever a change in phase is anticipated, such that the relative error in response quantities is always smaller than $10^{-10}$.

After the response quantities are determined, the integrals in the energy equation (24) are evaluated by integrating the expressions in the energy equation using a suitable integration technique [21]. During evaluation, comparing the left and right-hand side of Equation (25) can check accuracy of the integration.

## 4. EXAMPLE SYSTEM

A single-storey structure isolated by VFPI has been considered for evaluating the effectiveness of the proposed isolator. Different parametric studies have been carried out for the structure subjected to NS component of 1940 El Centro ground motion. The results are compared with that of the same structure isolated using FPS with isolator period equal to the initial time period (at zero sliding displacement) of the VFPI. Some results have also been compared to that of the example structure isolated using PF isolator. The El Centro ground motion has peak ground acceleration (PGA) of $0.319g$, peak ground velocity (PGV) of 0.36 m/s and peak ground displacement (PGD) of 0.2134 m. The analyses have been carried out for three scaled intensities of the recorded ground motion: $0.5 \times$ El Centro (low intensity), $1.0 \times$ El Centro (medium intensity) and $2.0 \times$ El Centro (high intensity), corresponding to peak ground accelerations of $0.160g$, $0.319g$, and $0.638g$, respectively.

The behaviour has been studied through the time history of response, response spectra and energy spectra. The response spectra have been defined as the plots of peak response quantities versus the parameter under consideration. Different definitions of energy spectra for fixed-base structures have been proposed in the literature [22, 23, 26]. In isolated systems, the recoverable energy that is actually transmitted to the structure is important. So, input energy spectra and recoverable energy (kinetic energy + potential energy) spectra have been defined as the corresponding peak energy during the earthquake ground motions.

The mass of the structure and base are taken equal, so that the mass ratio is 0.5. Stiffness of the structure is taken such that the time period of fixed-base structure is 0.5 s, while its damping ratio is taken as 2 per cent of critical value. Unless specified otherwise, VFPI with FVF of 10 ($d = 0.1$ m) has been considered. The initial time period of 2.0 s is chosen for VFPI for all the investigations. For comparison, the example FPS is also taken with its time period of 2.0 s.

### *4.1. Time-history response*

The time history of absolute acceleration response of example single-storey structure on VFPI subjected to El Centro ground motion scaled to twice intensity is shown in Figure 6(a). This high-intensity earthquake is chosen to show that the VFPI incorporates the advantages of both FPS and PF systems. The comparison of the response of system with FPS clearly shows that the structure with VFPI experiences significantly lower acceleration. Interestingly, the accelerations in VFPI and PF systems are similar since the maximum force transmitted at the sliding surface is bounded in both systems, leading to fail-safe behaviour even under very large excitations. The

 

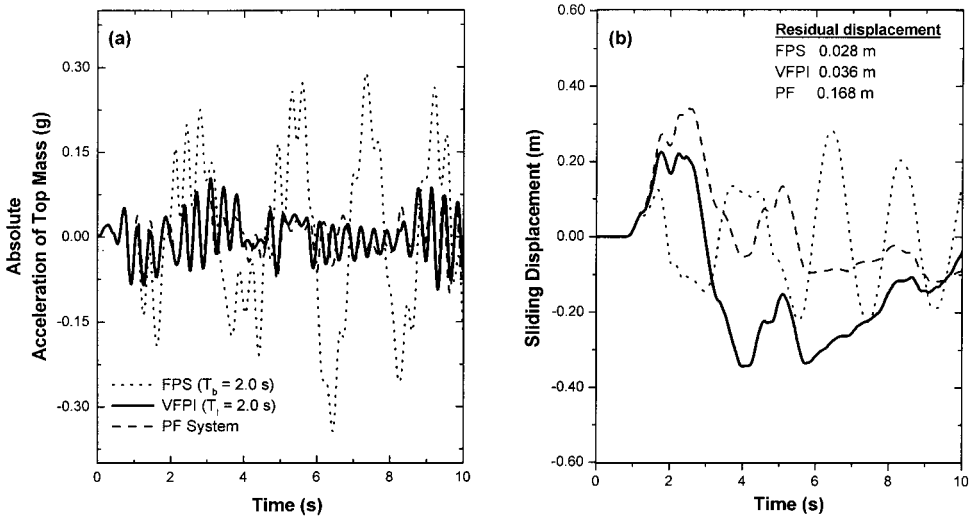


Figure 6. Typical response time-history plots for example SDOF structure subjected to El Centro 1940 (NS) ground motion scaled by factor 2 ($\mu = 0.02$, $\alpha = 0.5$, $\xi_0 = 2\%$).

time history of sliding displacement [Figure 5(b)] shows all three systems with similar maximum displacements. However, the residual displacement for PF system is very large while those for FPS and VFPI systems are significantly lower, clearly demonstrating their ability to restore the structure to its original position.

Time history of absolute input energy and the recoverable energy transmitted to the structure are shown in Figure 7. From these plots it is seen that there is a substantial reduction in both the absolute input energy and the energy transmitted to the structure for system with VFPI in comparison with that of FPS. This is due to the fact that the force transmitted by the PF and VFPI systems are much smaller than that by FPS. The softening mechanism of VFPI further significantly reduces the maximum energy imparted for high levels of excitations.

### *4.2. Effect of isolator geometry*

The geometrical properties of the sliding surface are completely defined by parameters $b$ and $d$. If the initial isolator frequency is fixed (governed by the ratio $b/d^2$), the geometry is defined by the frequency variation factor (FVF). A very low value of FVF results in a performance similar to FPS (almost constant isolator period), while a very high value results in performance similar to PF system. The appropriate value of FVF will combine the advantages of both resulting in robust isolator performance. To study the effect of FVF on the response quantities, the example structure isolated with VFPI is analysed for the different intensities of El Centro earthquake. Figure 8 shows the spectra of response for different FVF when the initial time period of the isolator is taken as 2.0 s.

From the response it can be observed that the variation of FVF has negligible effect on the peak response quantities for low-intensity earthquakes. This is primarily because the sliding displacements are very small, and the effect of variation in the isolator geometry is negligible.

 

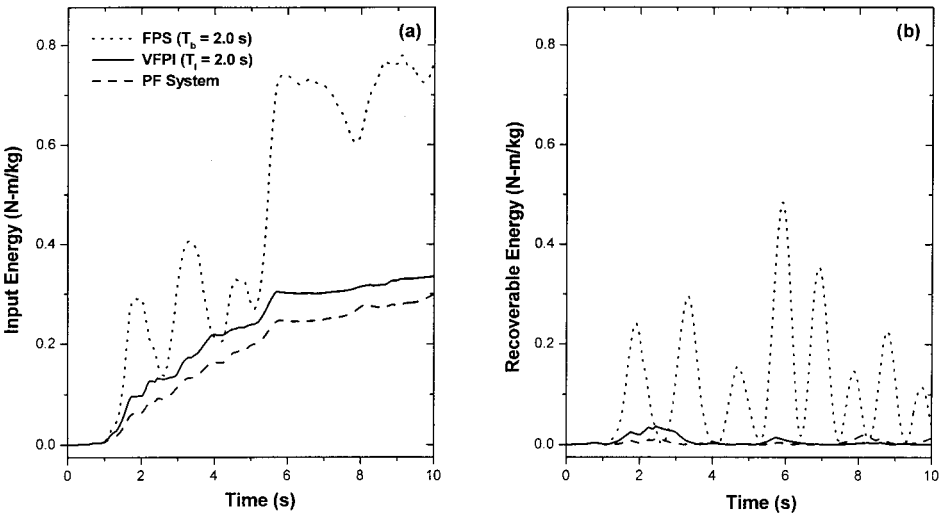


Figure 7. Typical energy time-history response of example SDOF structure subjected to El Centro 1940 (NS) ground motion scaled by factor 2 ($\mu = 0.02$, FVF = 10, $\alpha = 0.5$, $\xi_0 = 2\%$).

In this situation, the VFPI behaves similar to FPS with oscillation period equal to the initial time period of VFPI. However there may be a marginal increase in the sliding and residual displacements for very high value of FVF, wherein the isolator behaves similar to PF system.

The results for medium and high-intensity earthquake in Figure 8 show that the effect of FVF may be significant for high-intensity earthquake. When FVF is increased, the absolute acceleration decreases while the sliding displacement increases. This implies that it is possible to reduce the accelerations transmitted to the structure under high intensity of excitations by increasing the rate of variation of the isolator frequency. However, if the FVF is very large the residual displacements cannot be controlled [Figure 8(c)]. The performance of VFPI is much better than FPS under high-intensity excitation due to its force softening mechanism. Clearly, optimal values of FVF can be chosen for the example system wherein the accelerations and displacements are both within acceptable range.

The energy quantities are based on both displacement and acceleration responses, and can be used to better investigate the effectiveness of these isolators. The spectra showing variation of the energy input and recoverable energy with respect to FVF for different intensities of ground motion are shown in Figure 9. It is clearly seen that under high intensity ground motions, both the maximum input energy and maximum recoverable energy are significantly reduced for FVF larger than 2. However, these quantities remain practically unchanged for low- and medium-intensity earthquakes.

The energy spectra can be used to obtain more information about the characteristics of the VFPI. It can be seen that the input energy spectrum has a peak for high intensity of earthquake when FVF is around unity. The peak value of input energy is even larger than its value when FVF is very low (corresponding to FPS isolator). This is due to the restoring force characteristics of VFPI. The force at the isolator level in VFPI is limited to the sum of the peak restoring force,

 

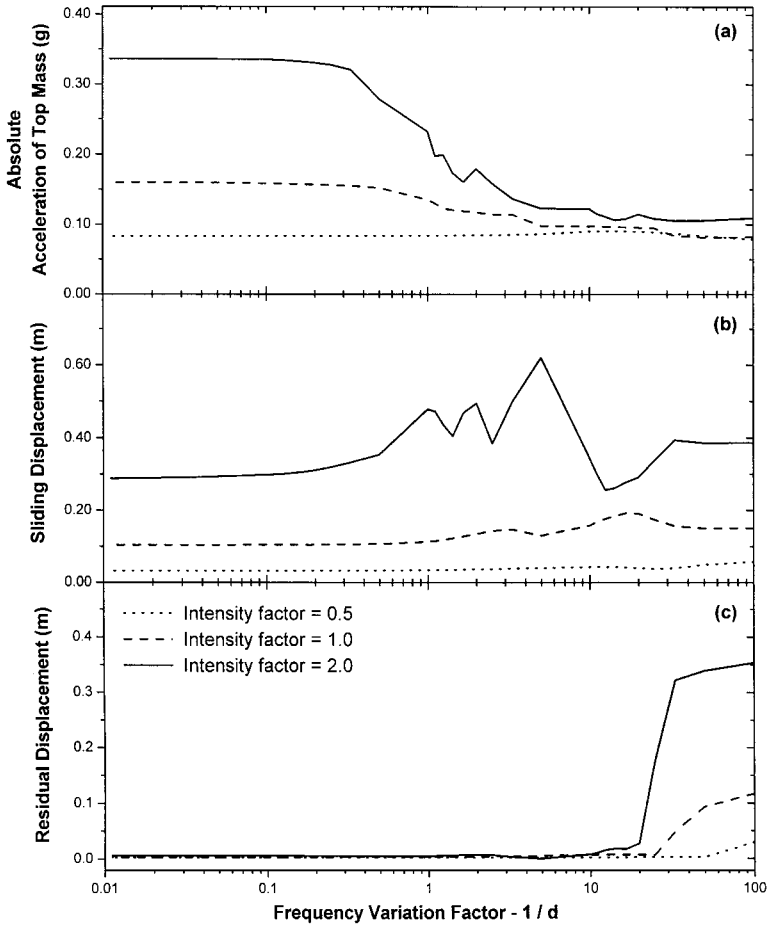


Figure 8. Effect of isolator geometry for scaled intensities of El Centro 1940 (NS) ground motion ($T_1 = 2.0$ s, $\mu = 0.02$, $\omega_0 = 2$ Hz, $\alpha = 0.5$, $\xi_0 = 2\%$).

which occurs at a sliding displacement of $0.58d$, and the frictional force. The peak restoring force increases with increase in the ratio $b/d$. As a result, the peak force increases with increase in $d$ (decrease in FVF) keeping $b/d^2$ constant; however, this occurs at large sliding displacements. The peak responses for excitations with intensity factor 2.0 have been given in Table I. It can be seen that for small values of $d$, although the maximum isolator displacement exceeds this peak value, the maximum restoring force transmitted is small. As the value of $d$ increases, the maximum restoring force that is transmitted increases. The peak energy will occur when both the force transmitted and the displacement are more. Till this value of FVF, the attainable peak restoring force is reached. But as these peak forces are less (due to small value of $d$), lesser accelerations are transmitted allowing higher sliding displacements. After this point the force transmitted is higher which helps to restrict the displacements and the energy again reduces. Although the peak occurs

 

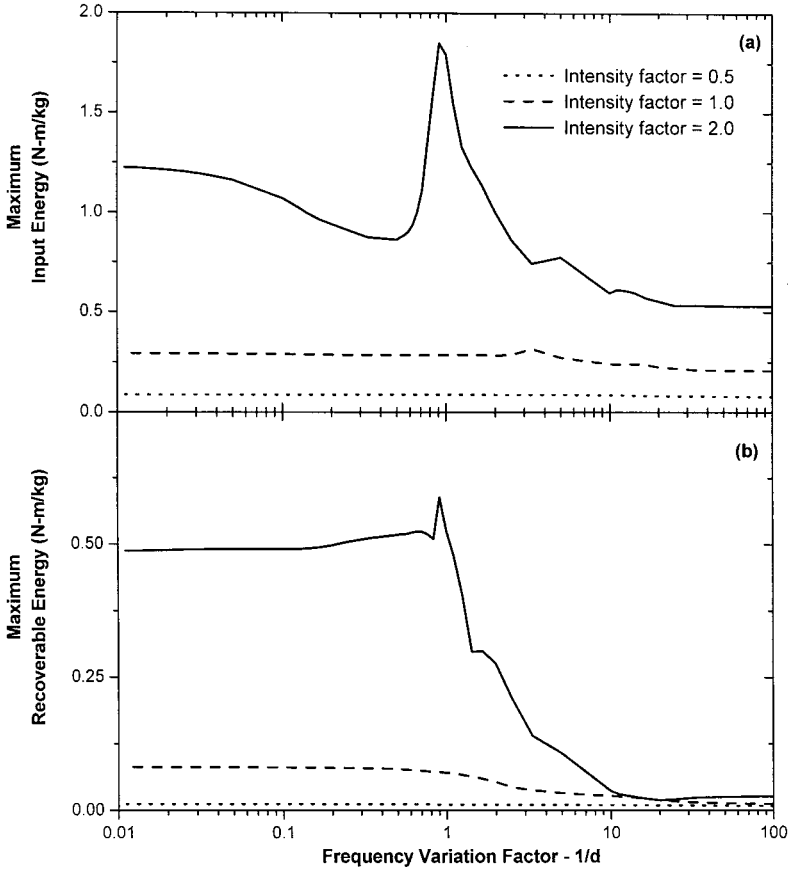


Figure 9. Effect of isolator geometry on peak energy quantities for scaled intensities of El Centro 1940 (NS) ground motion ($\mu = 0.02$, $T_1 = 2.0$ s, $\omega_0 = 2$ Hz, $\alpha = 0.5$, $\xi_0 = 2\%$).

in the input energy, it has a very little effect on the recoverable energy [Figure 9(b)] since this energy is dissipated by sliding friction.

Based on the above discussions of response and energy spectra, the criteria for choice of VFPI parameters should be low energy as well as small residual displacement. In view of this requirement, the practical range of FVF is recommended from 3 to 10 ($d = 0.10$–$0.33$ m).

### *4.3. Effect of coefficient of friction*

Depending on the choice of material for the sliding surface and the slider, a wide range of coefficient of friction can be obtained. The influence of coefficient of friction has been investigated by evaluating the performance of SDOF systems with VFPI with different coefficients of friction. For comparison purposes, the systems are also analysed with FPS and PF system with the same coefficient of friction. Since friction at the sliding surface results in loss of energy, the effect of coefficient of friction can be best studied through energy spectra.

 

Table I. Effect of isolator geometry on peak response quantities for high-intensity excitation ($\mu = 0.02$).

| $d$ (m) | Sliding displacement for maximum RF (0.58$d$) (m) | Maximum response | | |
|---|---|---|---|---|
| | | Restoring force | Acceleration ($g$) | Isolator displacement (m) |
| 0.5 | 0.290 | 0.0790 | 0.176 | 0.438 |
| 0.7 | 0.406 | 0.1106 | 0.191 | 0.525 |
| 0.9 | 0.522 | 0.1422 | 0.305 | 0.659 |
| 1.0 | 0.580 | 0.1580 | 0.336 | 0.765 |
| 1.1 | 0.638 | 0.1738 | 0.375 | 0.790 |
| 1.3 | 0.754 | 0.2012† | 0.332 | 0.573 |
| 1.5 | 0.870 | 0.2067† | 0.335 | 0.428 |
| 1.7 | 0.986 | 0.2123† | 0.333 | 0.385 |
| 1.9 | 1.102 | 0.2208† | 0.331 | 0.373 |
| 2.0 | 1.16 | 0.1921† | 0.331 | 0.369 |

† These peak forces are lower than the force at sliding displacement of 0.58$d$.

For the example systems, the VFPI has initial time period of 2.0 s ($b = 0.01$ m and $d = 0.10$ m) and FPS has constant time period of 2.0 s ($R = 1.0$ m). The coefficients of friction between 0.01 and 0.10 have been considered. The spectra of input energy and recoverable energy are shown in Figure 10. The energy spectra for the low-intensity earthquake show that behaviour is almost independent of coefficient of friction.

For the high-intensity excitations (intensity factor = 2.0), it is observed that the input energy for FPS initially decreases marginally with increase in coefficient of friction, reaches a minimum value, and then increases for higher coefficient of friction. This is due to the variation in the maximum isolator force transmitted for different coefficients of friction. For high coefficient of friction the increase in energy is due to the high frictional force (lesser sliding displacements) and for very low coefficient of friction, the increase in energy is due to high restoring force (higher sliding displacement). In contrast to this, for VFPI and PF systems the input energy monotonically increases with increase in coefficient of friction. The behaviour of VFPI is similar to that of PF system due to the softening of restoring force in VFPI at large sliding displacement.

The portion of input energy that is not dissipated through friction is transmitted to the structure as recoverable energy. The spectra of maximum recoverable energy are also shown in Figure 9, clearly showing the difference in performance of FPS and VFPI. As has been discussed earlier, the FPS behaves primarily as energy dissipator; on the other hand, the VFPI is effective both as energy dissipator and isolator. When the coefficient of friction is low, less energy is dissipated in FPS and the maximum recoverable energy in the structure is large. In contrast, the energy transmitted steadily decreases with lower coefficient of friction in case of both VFPI and PF system.

The spectra of maximum sliding and residual displacements for VFPI, FPS and PF systems are shown in Figure 11. It is found that for coefficient of friction greater than 0.02, the displacement response of both VFPI and FPS are significantly better than that of PF system. Although the sliding displacement of VFPI is larger than that of FPS, the residual displacements are similar and are significantly less than that of PF systems. This implies that VFPI judiciously combines the advantages of FPS and PF system.

 

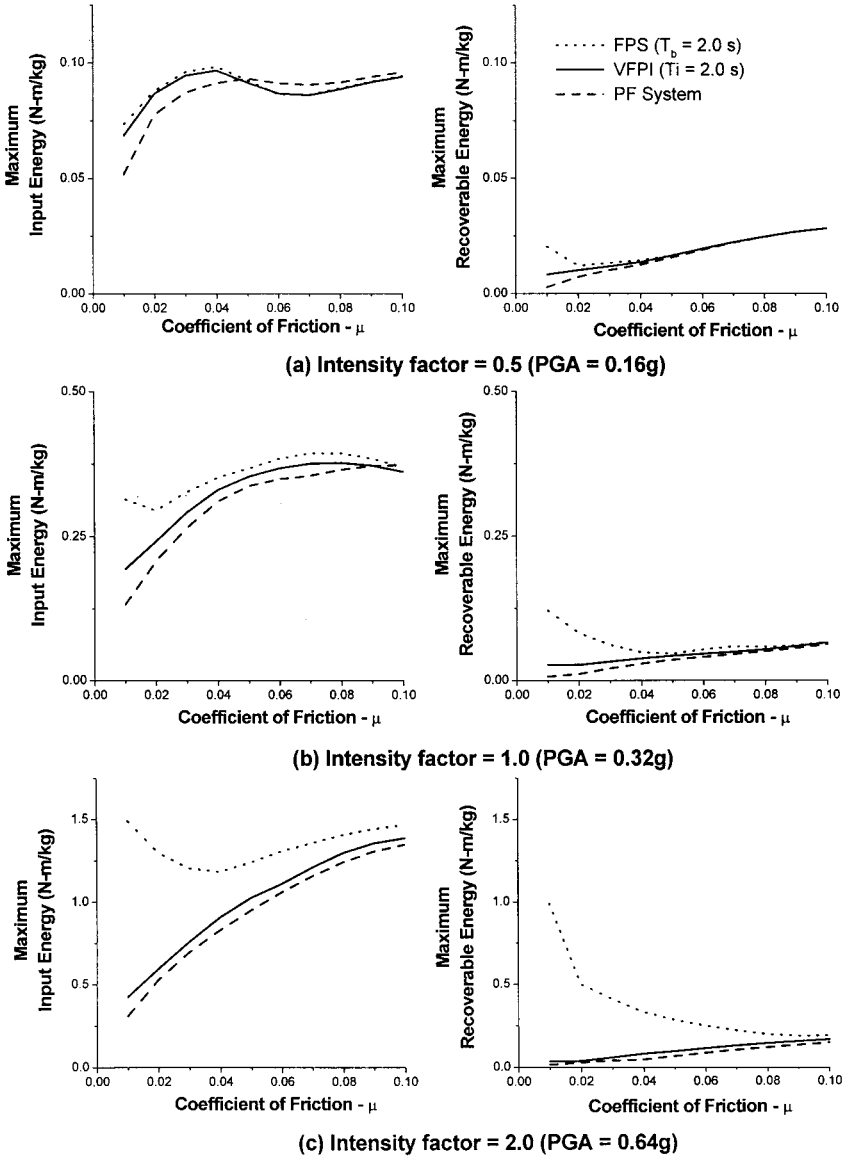


Figure 10. Effect of coefficient of friction on peak energy quantities for scaled intensities of El Centro 1940 (NS) ground motion ($T_b = 2.0$ s, $T_1 = 2.0$ s, FVF = 10, $\omega_0 = 2.0$ Hz, $\alpha = 0.5$, $\xi_0 = 2\%$).

### 4.4. *Influence of structural flexibility*

The isolation systems are robust and practically useful when they are effective for different structures with wide range of properties. For dynamic response, the most important property is the fundamental time period of the structure. For most typical building structures, the

 

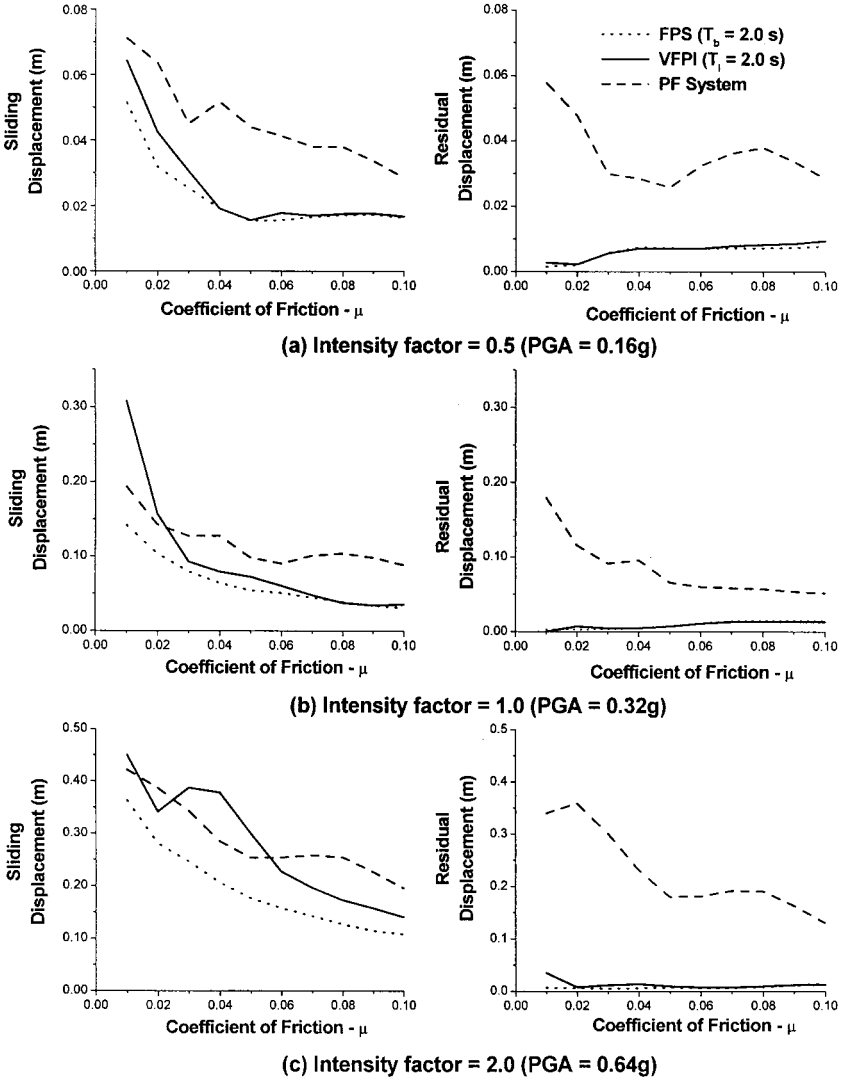


Figure 11. Effect of coefficient of friction on displacement response for scaled intensities of El Centro 1940 (NS) ground motion ($T_b = 2.0$ s, $T_I = 2.0$ s, $\omega_0 = 2.0$ Hz, $\alpha = 0.5$, $\xi_0 = 2\%$).

fundamental time period varies between 0.1 to 0.5 s. Tall buildings and flexible structures such as bridges have periods of up to 2 s or longer. Base isolator derives its effectiveness by increasing the time period of the structure. It is therefore essential that the fundamental time period of the structure be shorter than the time period of the isolator. In this investigation, the time period of the isolators is chosen as 2.0 s, and a wide range of structural time period from 0.1 to 2.0 s has been considered. These choices correspond to the most likely practical values of these parameters.

 

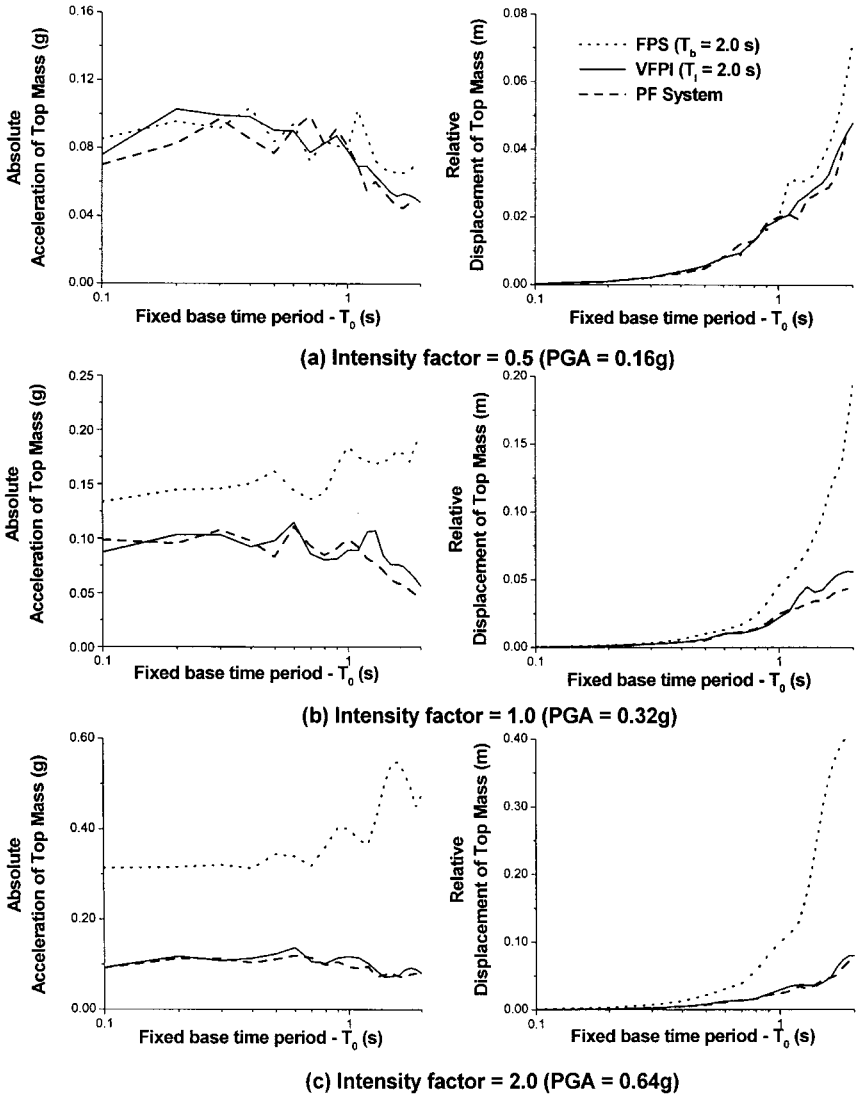


Figure 12. Effect of structural time period on peak response quantities for scaled intensities of El Centro 1940 (NS) ground motion ($T_b = 2.0$ s, $T_i = 2.0$ s, $\mu = 0.02$, $\alpha = 0.5$, $\xi_0 = 2\%$).

The response quantities of interest are acceleration and displacement of the structure, and the input and recoverable energies in the system. The spectra for absolute acceleration and relative displacement of the structure mass are shown in Figure 12 for different intensities of El Centro ground motions. It is observed that for low intensity of excitations the behaviour of all three isolators is similar, and the maximum acceleration is relatively independent of the structure time period.

 

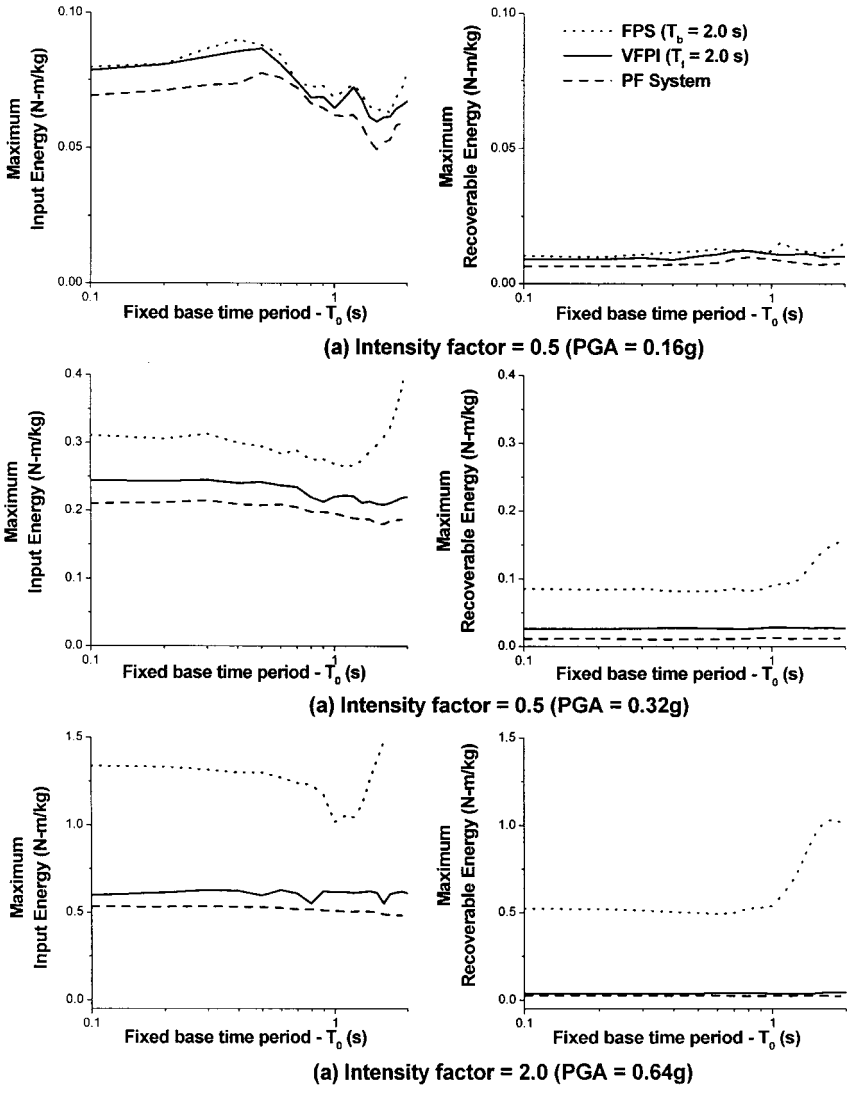


Figure 13. Effect of structural period on peak energy quantities transmitted to the structure for scaled intensities of El Centro 1940 (NS) ground motion ($T_b = 2.0$ s, $T_1 = 2.0$ s, FVF = 10, $\mu = 0.02$, $\alpha = 0.5$, $\xi_0 = 2\%$).

When the structure is subjected to higher intensity of base excitations, both the maximum displacement and acceleration of the structure are significantly higher when FPS is used. It can also be observed that the response of the structures with VFPI and PF systems is almost identical. Moreover, this behaviour is found consistent for all time periods of the structure. It is also seen that the response of structure with FPS increases for higher time periods, whereas the response of

 

VFPI is almost independent of the structural time period. This clearly shows that response of structure with VFPI is independent of both the amplitude and frequency content of excitation thereby preserving the most significant advantage of PF system.

The behaviour of structures with VFPI can be better understood from the energy spectra shown in Figure 13. Both the maximum input and recoverable energy spectra show that the behaviour of VFPI is similar to that of FPS for low-intensity excitations, and similar to that of PF system for high-intensity excitations. For intermediate intensity, the energy spectra are close to that of PF system, and indicate performance significantly superior to that of FPS isolator. It is also clear from these results that VFPI remains very effective for the fundamental time period of the structure between 0.1 to 2.0 s.

## 5. DISCUSSIONS AND CONCLUSIONS

A new sliding-type isolation system, variable frequency pendulum isolator, has been proposed and its effectiveness has been investigated for a wide range of structural, isolator and ground motion characteristics. The investigation has focused on two main aspects governing its effectiveness: (1) isolation, and (2) energy dissipation. Response and energy formulations similar to that for fixed-base structure have been developed in order to obtain better understanding of the system behaviour. The effectiveness of VFPI has been compared with that of FPS and PF system under similar conditions.

From the investigations presented herein, it is observed that VFPI acts as a combination of base isolator and energy dissipator. The VFPI thus combines the advantages of both FPS and PF system. It is also found that VFPI behaviour is stable at low intensity of excitations (as a high initial stiffness can be chosen). Furthermore, due to its force-softening characteristics, VFPI provides a fail-safe mechanism at high intensity of excitations without losing the ability to restore the structure close to its initial position. The advantage of variable frequency of oscillation is particularly significant for sliding surfaces with low coefficients of friction and during high intensity earthquakes. Even when very flexible structures are isolated (time period exceeding 0.5 s), the VFPI is found to be as effective as PF system.

Based on this investigation the following conclusions can be drawn.

1. The conventional isolation systems using pure friction and friction pendulum system have many limitations, and are effective only for certain structural and excitation parameters.
2. A new isolation system, variable frequency pendulum isolator (VFPI) has been proposed. VFPI is effective at all intensities of excitations, and for a wide variety of structure and isolator properties.
3. The VFPI behaviour is similar to that of FPS for low-intensity earthquake excitation, and similar to that of PF system for high-intensity earthquake excitation. So, VFPI can be designed to combine the advantages of both FPS and PF system.
4. The oscillation frequency of VFPI decreases sharply with increase in sliding displacement. As a result, the dominant frequency of excitation and the isolator frequency are not likely to tune. This property of frequency separation combined with force-softening mechanism of VFPI makes the isolator performance independent of both amplitude and frequency of excitations.

 

5. Energy evaluation of the structural system is very useful for understanding the mechanics of the system behaviour. The energy characteristics must be included in the criteria for determining the parameters of the isolator.

## APPENDIX A

The closed-form expressions that are required to carry out step-by-step integration of the equations of motion in both sliding and non-sliding phase have been presented below.

### *A.1 Non-sliding phase*

Expressing the ground excitation as a piece-wise linear function

$$\ddot{x}_g(t) = \beta_i \tau + a_i \tag{A.1}$$

where $\beta_i = (a_{i+1} - a_i)/(t_{i+1} - t_i)$ and $\tau = t - t_i$ with $t_i < t < t_{i+1}$. The modal equation for $m$th mode is given by

$$\ddot{y}_m + 2\xi_m \omega_m \dot{y}_m + \omega_m^2 y_m = -\gamma_m(\beta_i \tau + a_i), \quad m = 1, \ldots, n \tag{A.2}$$

where $y_m$ are the modal co-ordinates, $\omega_m$ is the modal frequency, $\xi_m$ is the modal damping and $\gamma_m$ is the modal participation factor. Using Duhamel's integral the final step-by-step algorithm can be written as

$$\begin{Bmatrix} y_{m_{i+1}} \\ \dot{y}_{m_{i+1}} \end{Bmatrix} = \begin{bmatrix} P_{11} & P_{12} \\ P_{21} & P_{22} \end{bmatrix} \begin{Bmatrix} y_{m_i} \\ \dot{y}_{m_i} \end{Bmatrix} + \begin{bmatrix} Q_{11} & Q_{12} \\ Q_{21} & Q_{22} \end{bmatrix} \begin{Bmatrix} a_i \\ a_{i+1} \end{Bmatrix} \tag{A.3}$$

where

$$P_{11} = e^{-\xi_m \omega_m \delta t_i}\left(\cos \omega_{m_d} \delta t_i + \frac{\xi_m}{\sqrt{1-\xi_m^2}} \sin \omega_{m_d} \delta t_i\right), \quad P_{12} = \frac{e^{-\xi_m \omega_m \delta t_i} \sin \omega_{m_d} \delta t_i}{\omega_{m_d}}$$

$$P_{21} = -\frac{\omega_m e^{-\xi_m \omega_m \delta t_i} \sin \omega_{m_d} \delta t_i}{\sqrt{1-\xi_m^2}}, \quad P_{22} = e^{-\xi_m \omega_m \delta t_i}\left(\cos \omega_{m_d} \delta t_i - \frac{\xi_m}{\sqrt{1-\xi_m^2}} \sin \omega_{m_d} \delta t_i\right)$$

$$Q_{11} = e^{-\xi_m \omega_m \delta t_i}\left\{\left(\frac{2\xi_m}{\omega_m^3 \delta t_i} + \frac{1}{\omega_m^2}\right)\cos \omega_{m_d} \delta t_i + \left(\frac{2\xi_m^2 - 1}{\omega_m^2 \delta t_i} + \frac{\xi_m}{\omega_m}\right)\frac{\sin \omega_{m_d} \delta t_i}{\omega_{m_d}}\right\} - \frac{2\xi_m}{\omega_m^3 \delta t_i}$$

$$Q_{12} = -e^{-\xi_m \omega_m \delta t_i}\left\{\left(\frac{2\xi_m}{\omega_m^3 \delta t_i}\right)\cos \omega_{m_d} \delta t_i + \left(\frac{2\xi_m^2 - 1}{\omega_m^2 \delta t_i}\right)\frac{\sin \omega_{m_d} \delta t_i}{\omega_{m_d}}\right\} + \frac{2\xi_m}{\omega_m^3 \delta t_i} - \frac{1}{\omega_m^2}$$

$$Q_{21} = -\frac{P_{11} - 1}{\omega_m^2 \delta t_i} - P_{12}, \quad Q_{22} = -Q_{21} - P_{12} \quad \text{and} \quad \omega_{m_d} = \omega_m \sqrt{1-\xi_m^2}$$

 

Knowing the modal co-ordinates the nodal deformations can be determined from the modal transformations.

*A.2 Sliding phase*

Here, the solution is got by a state-vector approach. The structure matrices are developed for the $n$ superstructure modes plus one base DOF. These $n+1$ DOFs are transformed to a state vector $\mathbf{u}$ consisting of $2(n+1)$ co-ordinates. Applying the complex modal analysis to this set of equations, they can be uncoupled equations. With the ground acceleration replaced by a piece-wise linear function the modal equation in this phase for the $m$th mode is

$$\dot{z}_m - \lambda_m z_m = -p_{g_m}(\beta_i \tau + a_i) - p_{f_m}\mu_f, \quad m = 1, \ldots, 2(n+1) \tag{A.4}$$

In the above equation the $z_m$ is the complex modal co-ordinate, $\lambda_m$ is the complex eigenvalue $p_{g_m}$ and $p_{f_m}$ are the complex participation factors for ground excitation and frictional force respectively and $\mu_f$ is the total frictional force. Integrating the above equation and putting $\tau = \delta t_i$ a step-by-step scheme for the solution at successive time steps can be written as

$$\begin{aligned} z_m(t_{i+1}) &= [z_m(t_i) - A_2]e^{\lambda_m \delta t_i} + A_1 \delta t_i + A_2 \\ \dot{z}_m(t_{i+1}) &= \lambda_m [z_m(t_i) - A_2]e^{\lambda_m \delta t_i} + A_1 \end{aligned} \qquad m = 1, \ldots, 2\,(n+1) \tag{A.5}$$

where

$$A_1 = \frac{p_{g_m}\beta_i}{\lambda_m}$$

$$A_2 = \frac{p_{g_m}\beta_i}{\lambda_m^2} + \frac{p_{g_m}a_i + p_{f_m}\mu_f}{\lambda_m}$$

Knowing the complex modal co-ordinates, the state vector $\mathbf{u}$ can be obtained from back-transformation of normal modal co-ordinates of the superstructure. Again the co-ordinate transformation for the normal co-ordinates can be used to get the nodal deformations.

## REFERENCES

1. Snowdem JC. Vibration isolation: use and characterisation. *NBS Handbook 128*, US National Bureau of Standards, MD, U.S.A., 1979.
2. Kelly JM. Aseismic base isolation: review and bibliography. *Soil Dynamics and Earthquake Engineering* 1986; **5**:202–216.
3. Kelly JM. State-of-the-art and state-of-the-practice in base isolation. *Seminar on Seismic Isolation, Passive Energy Dissipation and Active Control* (*ATC-17-1*), Applied Technology Council, Redwood City, CA, U.S.A., 1993.
4. Buckle IG, Mayes RL. Seismic isolation: history, application and performance — a world view. *Earthquake Spectra* 1990; **6**:161–201.
5. Mostaghel N, Hejazi M, Tanbakuchi J. Response of sliding structures to harmonic support motion. *Earthquake Engineering & Structural Dynamics* 1983; **11**:355–366.
6. Mostaghel N, Tanbakuchi J. Response of sliding structures to earthquake support motion. *Earthquake Engineering & Structural Dynamics* 1983; **11**:729–748.

 

7. Mokha A, Constantinou MC, Reinhorn AM. Teflon bearings in seismic base isolation: experimental studies and mathematical modelling. *Report No. NCEER-88-0038*, National Centre for Earthquake Engineering Research, State University of New York, Buffalo, NY, U.S.A., 1988.
8. Mokha A, Constantinou MC, Reinhorn AM. Teflon bearings in base isolation I: testing. *Journal of Structural Engineering* ASCE 1990; **116**(2):438–454.
9. Kelly JM. Base isolation in Japan, 1988. *Report No. UCB/EERC-38/20*, Earthquake Engineering Research Centre, University of California, Berkeley, CA, U.S.A., 1988.
10. Chalhoub MS, Kelly JM. Sliders and tension controlled reinforced bearings combined for earthquake isolation system. *Earthquake Engineering & Structural Dynamics* 1990; **19**:333–358.
11. Mostaghel N, Khodaverdian M. Dynamics of resilient friction base isolator (R-FBI). *Earthquake Engineering & Structural Dynamics* 1987; **15**:379–390.
12. Zayas VA, Low SS, Mahin SA. The FPS earthquake resisting system: experimental report. *Report No. UCB/EERC-87/01*, Earthquake Engineering Research Centre, University of California, Berkeley, CA, U.S.A., 1987.
13. Zayas VA, Low SS, Mahin SA. A simple pendulum technique for achieving seismic isolation. *Earthquake Spectra* 1990; **6**(2):317–333.
14. Mokha A, Constantinou MC, Zayas VA. Experimental study of friction-pendulum isolation system. *Journal of Structural Engineering* ASCE, 1991; **117**(4):1201–1217.
15. Tsopelas P, Constantinou MC, Kim YS, Okamoto S. Experimental study of FPS system in bridge seismic isolation. *Earthquake Engineering & Structural Dynamics* 1996; **25**:65–78.
16. Tsai CS. Finite element formulations for friction pendulum seismic isolation bearings. *International Journal for Numerical Methods in Engineering* 1997; **40**:29–49.
17. Jose LR, Jaun CDL, Jose AI. Modelling aspects of structures isolated with friction pendulum system. *Earthquake Engineering & Structural Dynamics* 1998; **27**:845–867.
18. Wang YP, Chung LL, Liao WH. Seismic response analysis of bridges isolated with friction pendulum bearings. *Earthquake Engineering & Structural Dynamics* 1998; **27**:1069–1093.
19. Mokha A, Amin N, Constantinou MC, Zayas VA. Seismic isolation retrofit of a large historic building. *Journal of Structural Engineering* ASCE, 1996; **122**(3):298–308.
20. Sinha R, Pranesh M. FPS isolator for structural vibration control. *Proceedings of the International Conference on Theoretical, Applied, Computational and Experimental Mechanics*, Indian Institute of Technology, Kharagpur, India, 1998.
21. Pranesh M. VFPI: an innovative device for aseismic design. *Presynopsis Seminar Report*, Indian Institute of Technology, Bombay, India, 1998.
22. Uang CM, Bertero VV. Evaluation of seismic energy in structures. *Earthquake Engineering & Structural Dynamics* 1990; **19**:77–90.
23. Leger P, Dussault S. Seismic-energy dissipation in MDOF structures. *Journal of Structural Engineering* ASCE, 1992; **118**(5):1251–1269.
24. Pranesh M, Sinha R. Behaviour of multi-degree-of-freedom shear structure isolated using VFPI. *Proceedings of the Eighth Canadian Conference on Earthquake Engineering*, Canadian Association of Earthquake Engineering, Vancouver, BC, Canada, 1999.
25. Tsai HC, Kelly JM. Non-classical damping in dynamic analysis of base-isolated structures with internal equipment. *Earthquake Engineering & Structural Dynamics* 1988; **16**:29–43.
26. Zahrah TF, Hall WJ. Earthquake energy absorption in SDOF structures. *Journal of Structural Engineering* ASCE 1984; **110**(8):1757–1772.

 